Measurement 182 (2021) 109739

Contents lists available at ScienceDirect

Measurement

journal homepage: www.elsevier.com/locate/measurement

Retrieval of gas concentrations in optical spectroscopy with deep learning

Linbo Tian [a,c,1], Jiachen Sun [b,c,1], Jun Chang [a,b,c,*], Jinbao Xia [d,e], Zhifeng Zhang [b,c], Alexandre A. Kolomenskii [f], Hans A. Schuessler [f], Sasa Zhang [a,b,c,*]

[a] Key Laboratory of Education Ministry for Laser and Infrared System Integration Technology, Shandong University, 72 Binhai Road, Qingdao 266237, China
[b] School of Information Science and Engineering, Shandong University, 72 Binhai Road, Qingdao 266237, China
[c] Shandong Provincial Key Laboratory of Laser Technology and Application, Shandong University, 72 Binhai Road, Qingdao 266237, China
[d] State Key Laboratory of Crystal Materials, Shandong University, Jinan 250100, China
[e] The State Key Laboratory of Applied Optics, Changchun 130000, China
[f] Department of Physics and Astronomy, Texas A&M University, College Station, TX 77843-4242, USA

ARTICLE INFO

Keywords:
Direct Absorption Spectroscopy
Deep Neural Networks
Transfer learning
Gases Concentration Retrieval

ABSTRACT

A novel direct absorption spectroscopy gas sensing system based on end-to-end deep neural networks was proposed for measurements of gas concentration. One-dimensional convolutional neural network and deep multi-layer perceptron were explored to measure the concentrations of methane and acetylene. The accurate measurement results for both gases demonstrated that deep neural networks based direct absorption spectroscopy technique can be reliably applied to different gas molecules. The developed gas sensing system achieved more precise concentration retrieval compared with that of wavelength modulation spectroscopy, and fast computation speed as well as robustness to noisy conditions, laser aging and circuit parameter variation simultaneously. The combination of deep neural networks and direct absorption spectroscopy provides new ideas for the further research of gas absorption spectroscopy.

1. Introduction

Tunable diode laser absorption spectroscopy (TDLAS) has been developed and exploited by researchers for various applications that require gas sensing, such as industrial process emission monitoring [1–3], combustion field diagnosis [4–6], and breath analysis [7,8], because of its high sensitivity, fast response speed, non-invasive, and simple measurement system. Direct Absorption Spectroscopy (DAS) [9,10] and Wavelength Modulation Spectroscopy (WMS) [11–16] are the two most commonly used and representative technologies. Although the WMS has attracted wide attention owing to its effective noise suppression and enhanced robustness through detecting harmonic signals, the DAS is still unbreakable in various detection scenarios such as isotopic abundance computation [17], temperature [6] and concentration retrieval [9] because of its advantages of low-cost detection system and intuitive acquisition of absorption features.

However, the accuracy of DAS has always been limited by issues such as baseline fitting, background noise, and the derivation from absorbance profiles to concentrations. Some efforts have been made to solve these troublesome problems for the more accurate measurements. As the most important procedure in extracting absorption features, high-precision baseline fitting is required to ensure correct processing of DAS transmitted signal. Traditionally, the baseline is defined by directly fitting low-order polynomials of the data in the non-absorbing region. Du et al. proposed to use sine wave instead of triangular wave or sawtooth wave to reduce the bandwidth requirements of the detection system and simultaneously developed a time-domain fitting routine to derive the sinusoidal baseline for achieving high-precision measurement [18]. Zhou et al. developed a Kalman filter based on BP neural network to suppress background noise of gas absorption spectra and performed high precision on-line measurements [19]. In the study of Liu et al., wavelet denoising was utilized to preprocess the DAS transmitted signal. The performance of two algorithms, linear regression and neural network, in establishing the mapping relationship between absorbance profile and gas concentration, was compared [17]. Although Liu's method replaces the derivation from absorbance profiles to concentrations, the absorbance profile is still obtained by baseline fitting of the DAS transmitted signal. Obviously, the whole process, from baseline

* Corresponding authors at: School of Information Science and Engineering, Key Laboratory of Education Ministry for Laser and Infrared System Integration Technology, Shandong University, 72 Binhai Road, Qingdao 266237, China.
E-mail addresses: changjun@sdu.edu.cn (J. Chang), Sasazhang@sdu.edu.cn (S. Zhang).
[1] Linbo Tian and Jiachen Sun contribute equally to this work.

https://doi.org/10.1016/j.measurement.2021.109739
Received 17 March 2021; Received in revised form 18 May 2021; Accepted 7 June 2021
Available online 15 June 2021
0263-2241/© 2021 Elsevier Ltd. All rights reserved.

fitting to the concentration retrieval, is done or designed by human researchers at present, where the detection precision is inevitably restricted by manual intervention.

So far, deep learning (DL) has established state-of-the-art achievements in absorption and excitation spectroscopy [17,20], hyperspectral image classification [21–25], reconstruction of ultrashort pulses [26,27] and material discovery [28–30], consistently outperforming those techniques which use hand-crafted features. However, the efficiency of DL approaches is often questioned because the quality of training depends on the quantity of the dataset. In the field of gas absorption spectroscopy, it is extremely time-consuming and laborious to obtain the adequate data for deep learning training through experiments. Therefore, the limited experimental data are commonly used for training the models with simple structures, resulting in the limited detection accuracy. In this case such model is not suitable for the high sensitivity and precision detection of trace gases [17].

To address the above problems, we proposed our gas sensing technique with the deep neural networks (DNNs) to establish an end-to-end system which retrieves the DAS transmitted signal to the gas concentration directly without intermediate manual operation. Also, we exploited transfer learning to tackle the problem of limited number of experimental gas absorption spectra data. In this study two different gases were processed separately, and the accurate measurement results showed that the proposed technique could be reliably implemented to different gas molecules. We performed the quantitative comparison of our DNNs with three typical machine learning algorithms (MLs) (k-nearest neighbor, adaptive boost decision tree, decision tree) to prove the superiority of our DNNs. Besides, we compared the pre-trained DNNs that were fine-tuned on experimental data with the DNNs that were trained only on experimental data to verify the significance of transfer learning in improving model performance. The results indicated that the transfer learning scheme can effectively solve the dilemma of experimental data shortage. In addition, we compared the performance of our DNNs based DAS gas sensor and the state-of-the-art WMS technique. Without complicated system arrangement and high-speed electronics, the proposed technique achieved better performance than the WMS in an extremely short period of time (0.5 ms for each computation). Finally, the proposed technique can resolve the problem of laser ageing and optimize gas sensing systems to avoid the influence of different circuit parameters and light intensity variations, which reflects the prospect of engineering application of this technique. More specifically, the main contributions of this paper are three-fold:

1. The main contribution of this study is to establish a basis for further research on the contacts between the deep learning algorithms with trace gas diagnosis, blended absorption features identification and separation, and so on.
2. An end-to-end deep neural networks (DNNs) based direct absorption spectroscopy (DAS) gas sensing system is developed for methane and acetylene concentrations retrieval without intermediate manual intervention. The precise detection results of both gases as representative gases in chemical production, industrial monitoring as well as atmospheric monitoring indicating the feasibility of applications to other gas molecules.
3. We exploited the transfer learning to solve the problem of insufficient experimental data. We verified the significance of transfer learning by employing the Wilcoxon signed test between the transferred models and the models that were only trained over small experimental dataset.

The full implementation (our deep neural network architectures, pre-training and transfer learning) and the supplementary material (statistical test results) are available at https://github.com/Popsama/gas_retrieval_with_deep_learning.

The **section 2** discusses the design of the gas sensor. We explicate the results of the proposed technique in **section 3**. The conclusion and prospects for the future work are talked about in **section 4**.

2. Design of gas sensor

2.1. Spectral selection

TDLAS technology is based on the theory of molecular absorption spectroscopy. When a laser beam with an optical frequency ν and intensity I_0 passes through the gaseous medium to be analyzed, the beam will be absorbed due to stimulated optical transitions of gas molecules corresponding to the optical frequency ν. The incident optical intensity I_0, and the transmitted optical intensity I_t satisfy the Beer-Lambert law [31]:

$$\alpha(\nu) = -\ln\left[\frac{I_t(\nu)}{I_0(\nu)}\right] = S(T)\phi(\nu)Py_jL \tag{1}$$

Here $\alpha(\nu)$ is the absorbance, S(T) is the temperature-dependent line intensity of the transition, $\phi(\nu)$ is the normalized line-shape function of the molecular absorption, P is the pressure, y_j is the mole fraction (concentration) of the absorbing species j, and L is the pathlength.

In order to verify the feasibility of our proposed gas sensor based on DNNs applied in the various gas molecules, acetylene and methane were selected since their representativeness in chemical production, industrial monitoring as well as atmospheric monitoring. Based on HITRAN database [32], the absorption lines of acetylene and methane in the near-IR region are shown in Fig. 1. The absorption lines marked in red in Fig. 1 are the ones under study in this paper. They are the P(13) absorption line of acetylene near 6523.8792 cm^{-1} and the R(3) absorption line of methane near 6046.9636 cm^{-1}.

2.2. Sensor system configuration

Our experimental arrangement of DAS technology is shown in Fig. 2 **(a)** without the WMS unit. The two distributed feedback laser diodes (DFB-LDs) (BF14-DFB-1532, Wuhan 69 Sensor Technology, China and SWLD-165310S22-01, Allwave, China) were utilized to scan the absorption lines of acetylene and methane, respectively. The DFB-LDs were controlled by a driving module consisting of a home-made LD driver circuit and ARM7 (LPC1758, NXP, Netherlands), which was used to generate a ~ 1 Hz scanning ramp signal. The output beam of the DFB-LD was coupled into the optical fiber, and then transmitted to the fiber-coupled Herriott cell (300 cm path-length). 1000 sets of various concentrations (ranging from 0 to 1000 ppm) of methane and 1000 sets of various concentrations (ranging from 0 to 500 ppm) of acetylene gases were obtained by separately blending with nitrogen through a gas mixing dynamic distribution system (SFD-Y500, Nanjing Shuntai Technology, China), and were introduced into the Herriott cell. The output beam from the Herriott cell was converted to the DAS transmitted signals by a photodetector (BF14-PD300-F-N, Wuhan 69 Sensor Technology, China) and pre-amplifier in the photo-detector module. As the process shown in Fig. 2 **(b)**, the DAS transmitted signals were fed into the DNNs in a PC and the corresponding concentrations were directly retrieved.

The WMS technology was selected for simultaneous comparison with gas sensors based on DNNs. The arrangement of its experimental system is shown in Fig. 2(a), which includes the WMS unit. The two DFB-LDs were controlled by a driving module consisting of an ARM7, a signal generator (FY2300A, Feel Tech, China), and a home-made LD driver circuit. ARM7 was used to generate a ~ 1 Hz scanning ramp signal and the signal generator was used to generate a 2 kHz sinusoidal signal for modulation. The two signals were mixed at the adder as the driving signal for the DFB-LDs. The construction of the entire optical path and preparation of methane and acetylene gases were exactly the same as the DAS experimental system. In the demodulation part, a lock-in amplifier (HF2LI, Zurich Instruments, Zurich, Switzerland) with a reference signal of 4 kHz sinusoidal signal generated by the signal generator was

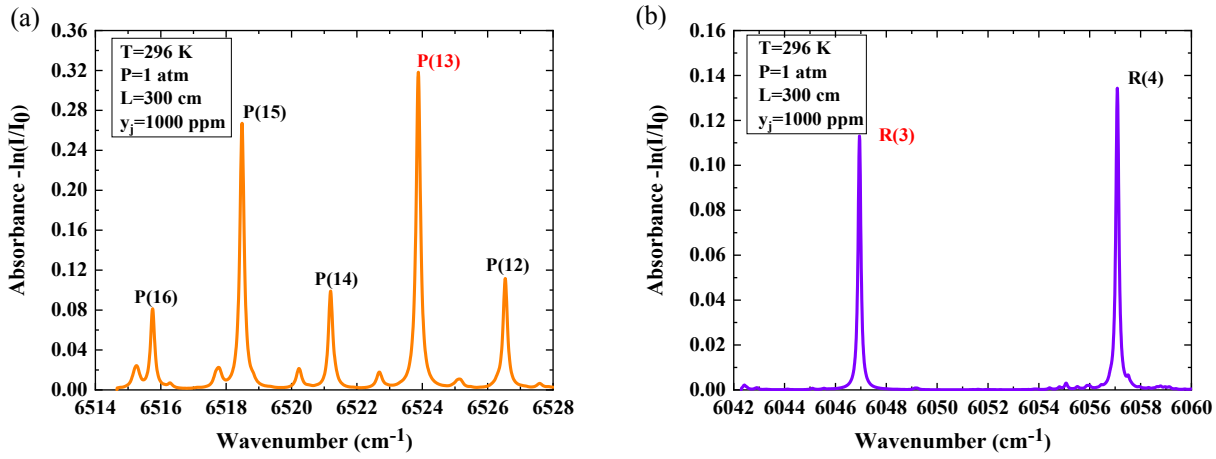

Fig. 1. The absorbance profiles of (a) acetylene and (b) methane under the conditions of y_j = 1000 ppm, T = 296 K, P = 1 atm, L = 300 cm.

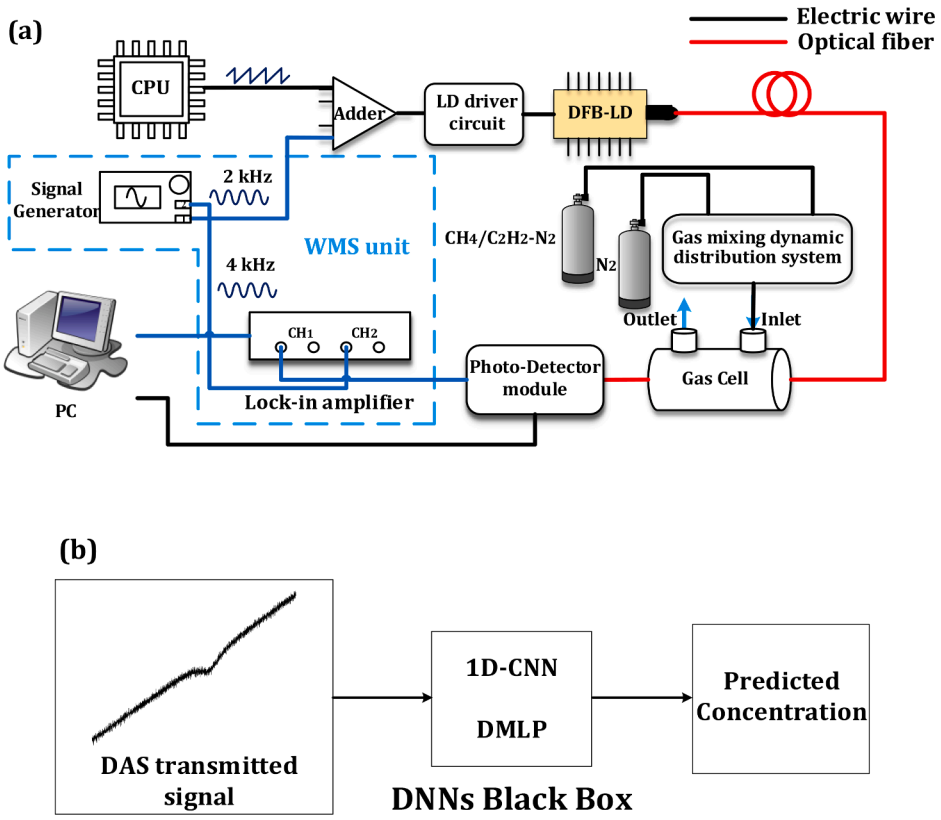

Fig. 2. (a) Schematic diagram of the experimental system. The DAS experimental system does not include the WMS unit, while the WMS system does. (b) Diagram of the retrieval process from the DAS transmitted signal to the predicted concentration. Our DNNs as a black box for predicting the concentration corresponding to the input DAS transmitted signal.

employed to extract the harmonic signals. The obtained second harmonic signals were processed in the PC to infer the corresponding concentrations.

2.3. The deep learning neural network construction

Here we introduce two neural network architectures illustrated in Fig. 3 and Fig. 4 to retrieve directly the gas concentrations from their corresponding DAS transmitted signal without baseline fitting and other manual process.

The 1D-CNN was designed as a convolutional blocks structure where each block consisted of two convolutional layer and a max-pooling layer. Such blocks transformed the input with learnt convolutional kernels in a convolutional layer and passed the output through a nonlinear pooling operation in a max-pooling layer. Several such blocks were stacked and the final output was obtained by flattening the output of the last global-average-pooling layer via the fully connected layers. The hyperparameters of our 1D-CNN is illustrated in Fig. 3.

The second DNNs model was based on the deep feedforward network (also called DMLP). The initial networks were composed of parameterized layers where the initialized parameters (or weights) were optimized via backpropagation algorithm with the goal of minimizing the loss function. Despite its architectural simplicity, the DMLP has been deployed in many scenarios because of its powerful universal

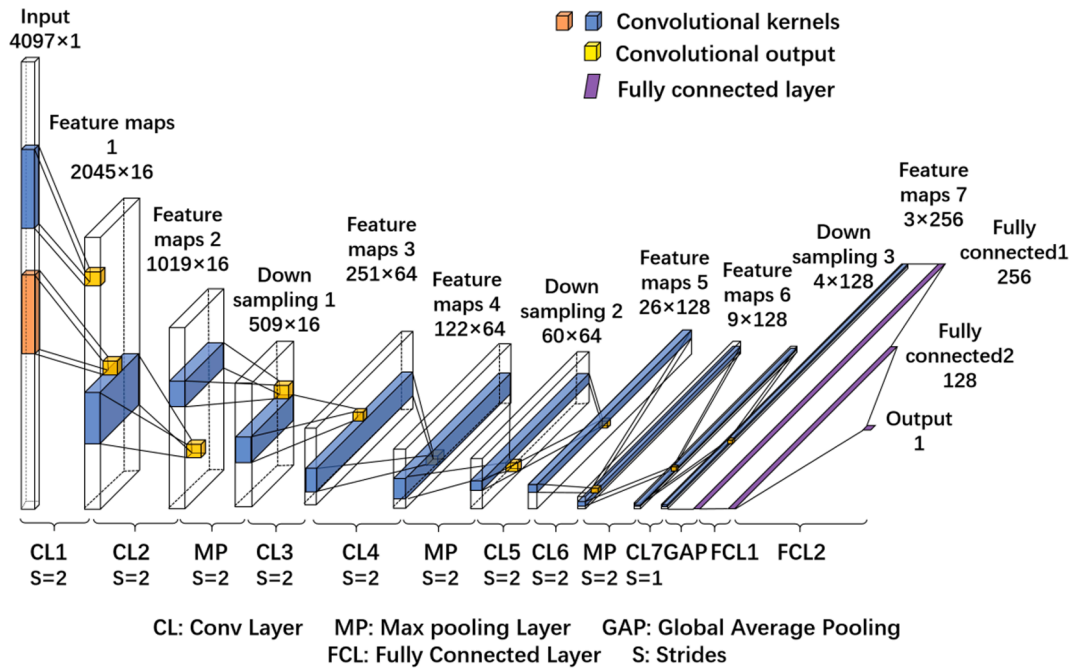

Fig. 3. The 1D-CNN architecture. The first 1D Conv layer comprises 16 kernels (the dimensions of (9, 1) applied to each kernel), so that 16 convolutional outputs can be produced. The dimensions of the input data fed into the first Conv layer is (4097, 1). The kernels will slide through the data for 2045 steps to conduct convolutional and activation operations, resulting in a (2045, 16) output. The second Conv layer with 16 kernels (dimensions of (9, 16)) results in the output with the dimensions (1019, 16). The max-pooling layer prevents overfitting of the learned features by taking the max value among multiple features and downsizing the size of the tensor to (504,16). The second and third Conv blocks were applied following the same concepts as the first block. The first dimension of kernels is still 9, while the second dimension doubled to be 64 and 128. The last Conv layer was connected to a global average pooling layer to decimate the dimensions to be (256, 1). The last two layers were fully-connected-layers (Dense layers). The output layer implements a sigmoid activation function rather than Relu to produce a concentration distribution within [0, 1].

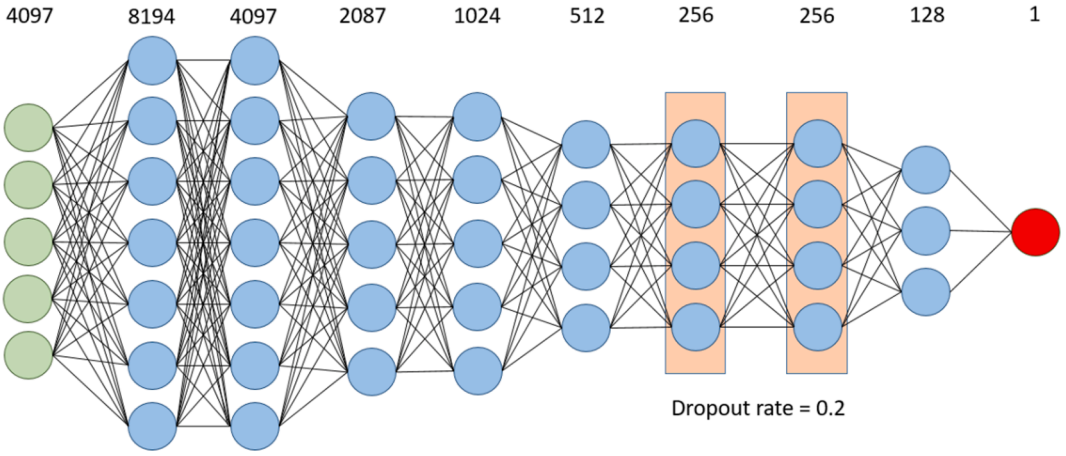

Fig. 4. The DMLP architecture. One input layer, 8 hidden layer and one output layer. The number of neurons in each layer are shown in figure. We added dropout operation in the 6-*th* and the 7-*th* hidden layer.

approximation. For more details about the DMLP architecture see Fig. 4.

We exploited the transfer leaning to overcome the dilemma of experimental data shortage, the whole scheme is shown in Fig. 5. First, we trained the DNNs over a source dataset which was composed of a large number of simulated DAS transmitted signals and their corresponding concentration ground truth, and then we fine-tuned the pre-trained models on a small experimental dataset to obtain the final model which can be well-generalizing under real data distribution. Specifically, we froze the weights of previous layers except the output layer of DNNs, only the weights of the output layer were optimized by the new data. The reason it works is that the initial layers focus on simple and generic features, while the deeper layers focus on more specific tasks, such as performing the concentration retrieval.

3. Experiments

3.1. Training and evaluation of concentration retrieval algorithms

3.1.1. A. Pre-training stage

The initial DNNs and MLs were first trained by simulated methane and acetylene data. To improve the robustness of the model in the presence of noise, we have enriched the diversity of gas concentrations (ranging from 0 to 1000 ppm, concentration interval is 0.1 ppm) under various SNR conditions (no noise, 10 dB, 15 dB and 20 dB). To get closer

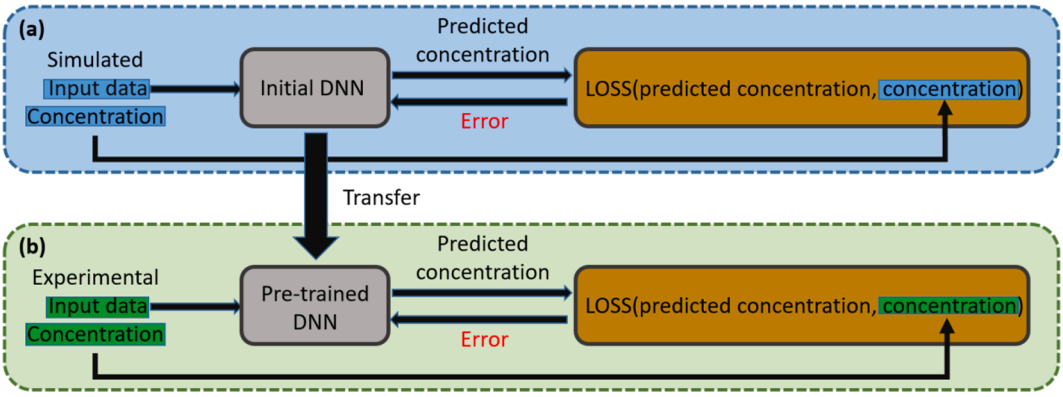

Fig. 5. Model training strategy (a) Pre-training stage, (b) Transfer learning stage.

to the experimental conditions, we set the ambient temperature at 296 K, the gas cell pressure of 1 atm, and the effective absorption optical path of 300 cm. 30,000 training samples, consisted of the pairs of inputs (transmitted signals) and labels (the corresponding ground truth concentrations), were collected for each gas during the pre-training stage. The ground truth concentrations were set in the simulation software.

Recent research [33,34] shows that the traditional cross validation (CV) or hold-out test tend to over-estimate the explorative prediction performance of machine learning models. K-fold cross validation is not only unable to effectively and accurately evaluate the exploration power of the models, but also unable to differentiate high explorative models from lower ones. Therefore, we used a data redundancy controlled cross validation method as reported in [33] to fix such problems. K-fold-forward cross validation (FCV) is a novel measure to more objectively evaluate the exploration power rather than interpolation power for the gas concentration retrieval models (the performed k-fold-forward cross validation scheme is illustrated in Fig. 6).

To conduct FCV, the dataset was first sorted by ascending concentration values and then split evenly into k subsets S_1, S_2, …, S_k. Concerning the first round, the models were trained on S_1 and the S_2 was set as validation set. In the next round, the models were trained on S_1 and S_2, and set the S_3 as validation set. This step was performed iteratively until all subsets were evaluated and the overall performance of all models was calculated. In this study, we experimented a series of k values ranging from 10 to 500 with step of 50. We set k to 100 for all the following experiments since the FCV results started oscillating within small limits when k was larger than 100.

We carried out an extensive search for the best DNNs architecture as well as in the hyper-parameters space. With respect to DMLP, we started from a two-layered architecture and incrementally increasing the depth to improve the learning capacity until a saturation point was reached. We explored with different combinations of the number of neurons units per layer. Two dropout layers were also added to avoid overfitting. The validation error converged at 9 layers (8 hidden layers and 1 output layer). Similarly, we experimented with a set of architectures for 1D-CNN. In addition, we started with a small range of values for each hyperparameter based on our intuition, rather than performing a grid search which would have been infeasible due to time and computational resource constraints. Learning rate values from 0.001 to 10^{-6} were tried. A search for dropout rate values ranging from 0.1 to 0.9 was carried for each of the two dropout layers. Other hyperparameters were also experimented in the same way. The best model architectures are shown in Fig. 3 and Fig. 4. The DNNs were implemented in Python 3.7 on a standard PC with a Nvidia Titan X GPU. The Keras framework [35] was employed to support the construction of DNNs (ADAM optimizer, learning rate of 10^{-5}, $\beta_1 = 0.9$, $\beta_2 = 0.999$, 2000 epochs).

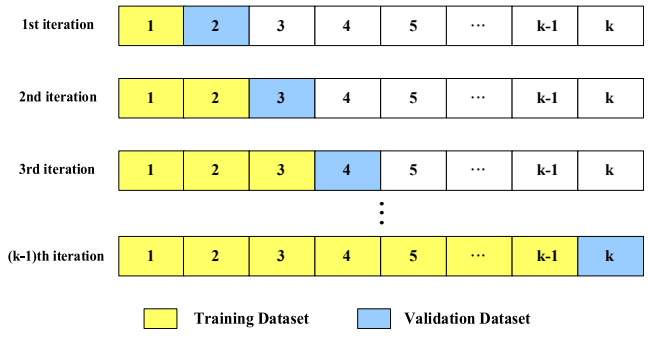

Fig. 6. Schematic representation of k-fold-forward cross validation.

By comparing the FCV results of all evaluated models, we can have an overview of the explorative power of our DNNs as well as traditional MLs. We performed the quantitative comparison of our DNNs with three typical machine learning algorithms (MLs) (k-nearest neighbor, adaptive boost decision tree, decision tree). We computed the absolute error (|ground truth-predicted concentration|) and the relative error (|ground truth-predicted concentration|/ground truth) as metrics to carry out the performance assessment. The FCV comparison results in terms of all models are shown in Table 1. Both DNNs proposed by us were significantly outperformed the MLs with respect to both gases. The best performance was achieved with the relative error of 0.1589% and the absolute error of 0.1167 ppm by DMLP while the worst performance belongs to DT with the relative error of 14.323% and the absolute error of 8.6788 ppm. In terms of absolute errors, the performance of our DNNs were an order of magnitude higher than that of the chosen machine learning models, which proved the superiority of our deep learning models.

4. B. Transfer learning stage

We employed transfer learning to fine-tune the DNNs that pre-trained over simulated data. As mentioned in the **section 2**, we adjusted the gas dynamic distribution system to produce mixed gases

Table 1
Performance evaluation of pre-training models. DT stands for decision tree regressor, ABDT stands for adaptive boosted decision tree regressor, KNN stands for K-nearest neighbor regressor.

	CH_4		C_2H_2	
	Relative errors (mean)/%	Absolute errors (mean)/ppm	Relative errors (mean)/%	Absolute errors (mean)/ppm
DT	14.323	8.6788	13.761	8.2202
ABDT	10.997	6.4236	10.792	6.4082
KNN	12.378	7.0836	12.029	7.0553
1D-CNN	0.2474	0.6591	0.2426	0.6029
DMLP	0.1589	0.1167	0.1216	0.1241

with different concentrations of CH_4 and C_2H_2 with buffer gas N_2. The configured gases were detected by our DAS system and 1,000 sets of methane and 1,000 sets of acetylene transmitted signals were experimentally collected as input data, while the preset gas concentrations of the mix gas dynamic distribution system were regarded as the labels (ground truth). The experimental data were also split into training set and validation set according to the FCV scheme for fine-tuning and evaluation of the models' performance. We compared the performance of (1) the DNNs trained only by the small number of experimental data and (2) the DNNs only pre-trained by simulated data without transfer learning and (3) the pre-trained DNNs in which transfer learning has been applied as shown in Table 2.

The positive effect of transfer learning is illustrated when comparing the PT + TF and TED. For both DNNs, the Wilcoxon signed rank tests were statistically significant at $p < 0.001$ for all 1D-CNNs and DMLPs, which indicating that the DNNs fine-tuned by the transfer learning significantly outperformed those trained only on the experimental data (Table 2). The observation results proved the importance of transfer learning to overcome the scarce experimental data problem and to help improve the models' performance on small experimental dataset. On the other hand, through transfer learning, the DNNs trained over simulated data allowed for obtaining the better generalization over the experimental dataset, in which the DMLPs got better performance than the 1D-CNNs, indicating that transfer learning improved DMLPs more significantly. In addition, the pre-trained models without being transferred on the experimental data (PT) achieved the worst performance, which was mainly due to the domain discrepancy between the simulated data distribution in ideal circumstance and the experimental data distribution in complex environment. This also explains why a small number of real experimental dataset is still needed, rather than completely using simulated data for training.

We further compared the performance of our DNNs with the typical MLs (see Table 2). When comparing the performance of the models that trained only on experimental data, although the performance of DNNs is not as good as that trained on a large simulated dataset, the performance of MLs is still worse. Besides, the transferred DNNs outperformed the MLs significantly ($p < 0.001$). In contrast with 1D-CNN, it is worth noting that the DMLPs trained only by experimental data performed worse in terms of both gases because of its large number of trainable weights that require large amounts of data to optimize. In this case, the reason for insufficient exploration capability of these MLs is due to its underlying mechanism, which is different from the reason for DMLPs. [33] explained this mechanism in details and showed that the DT, ABDT and KNN can be viewed as weighted neighborhoods schemes. By contrast, our DNNs show better exploration capability to predict validation samples outside the same domain as the training set.

To further evaluate the out-of-domain generalization performance of our DNNs, we introduced forward-holdout validation (FH) [33]. We sorted the experimental data by ascending the experimental dataset and then split it into training and validation sets in the proportion of 75% and 25%. Since the low concentration limit of detection is more concern in gas sensing, the pre-trained DNNs were fine-tuned on the 75% high concentration samples and tested on the 25% low concentration samples accordingly. In this way, we can evaluate whether the models that trained on the transmitted signals corresponding to high gas concentrations can correctly respond to the out of domain transmitted signals of low concentrations. Both figures in Fig. 7 shows that both models remain low errors in the training area while the test error increases gradually in the test area. Although the test error has an upward trend, it is still in the acceptable range compared with training error, which demonstrates that our DNNs meet the requirement for trace gas detection with a certain out-of-domain generalization ability. Furthermore, the error increases dramatically at extremely low concentration area where the weak transmitted signals corresponding to the low concentration are completely submerged in the system noise. In this case, it is encouraging that the models still controlled the prediction error of the noise dominated signals under 2 ppm. We plan to carry out the research of filtering algorithm in the future to improve the signal-to-noise ratio (SNR) of the system as well as the limit of detection for trace gases.

4.1. Evaluation of gas sensor

The spectroscopic sensor which consisted of DNNs-based concentration retrieval model and DAS-based hardware system was further evaluated and compared with the state-of-the-art WMS technique for the detection of both gases. We collected 15 typical concentrations for methane data ranging from 0 to 1000 ppm and for acetylene data ranging from 0 to 500 ppm, respectively. The concentration prediction comparison results are plotted in Fig. 8. Fig. 8**(a)** provides a global view and Fig. 8**(b)** shows more details of low concentration section. Concerning methane, the DNNs based sensor outperformed the WMS sensor especially in higher concentration region. On the other hand, the coefficients of determination (R^2) of DMLP based DAS sensor were higher than that of WMS setup for both gases, while 1D-CNN did slightly worse in terms of acetylene in low concentration region.

We made the error comparison analysis between WMS and the DNNs based DAS, as shown in Table 3. For both gases, DMLP based DAS techniques showed the best performance among all sensors (minimum absolute error and relative error). Both DNNs based DAS sensor achieved better results compared with WMS sensor in terms of methane. In the low concentration region of acetylene, the performance of 1D-CNN based DAS sensor suffered fluctuation due to the low SNR samples, in which it is difficult to extract features from noise. In addition, all the transferred models produced concentration retrieval computation within 0.5 ms, which is equivalent to 1/20 of the time required for DAS technology to complete the averaging of 10 k samples at a scanning frequency of 1 MHz [10].

To investigate the influence of laser aging on the proposed sensor system, the laser output light intensity was continuously attenuated to simulate the aging process. 500 ppm methane and 100 ppm acetylene were obtained by the gas mixing dynamic distribution system. By adjusting the optical attenuator, the laser output intensity was continuously reduced to 5% of the original intensity, while the transmitted signals were simultaneously fed into DNNs for concentration retrieval.

Table 2
FCV results of all schemes: PT + TF (pre-training + transfer learning), TED (Trained only on experimental data), PT (pre-trained models without transfer learning).

		CH_4			C_2H_2		
		R^2	Relative errors (mean)/%	Absolute errors (mean)/ppm	R^2	Relative errors (mean)/%	Absolute errors (mean)/ppm
1D-CNN	PT + TF	0.9858	0.6332	1.2523	0.9878	0.5848	1.0632
	TED	0.8723	5.7835	3.8923	0.8974	5.3082	3.4972
	PT	0.7223	12.7842	7.1783	0.7268	12.8063	7.0896
DMLP	PT + TF	0.9879	0.4675	1.0841	0.9890	0.4518	1.0274
	TED	0.8012	8.6792	5.8964	0.8038	8.6437	5.3944
	PT	0.6873	15.7892	9.7384	0.6881	15.3273	9.4672
DT	TED	0.6967	15.7648	8.9535	0.6922	15.6823	8.5129
ABDT	TED	0.7481	11.6210	6.7482	0.7682	11.4821	6.5723
KNN	TED	0.7043	13.1143	7.2893	0.7194	13.0385	7.0823

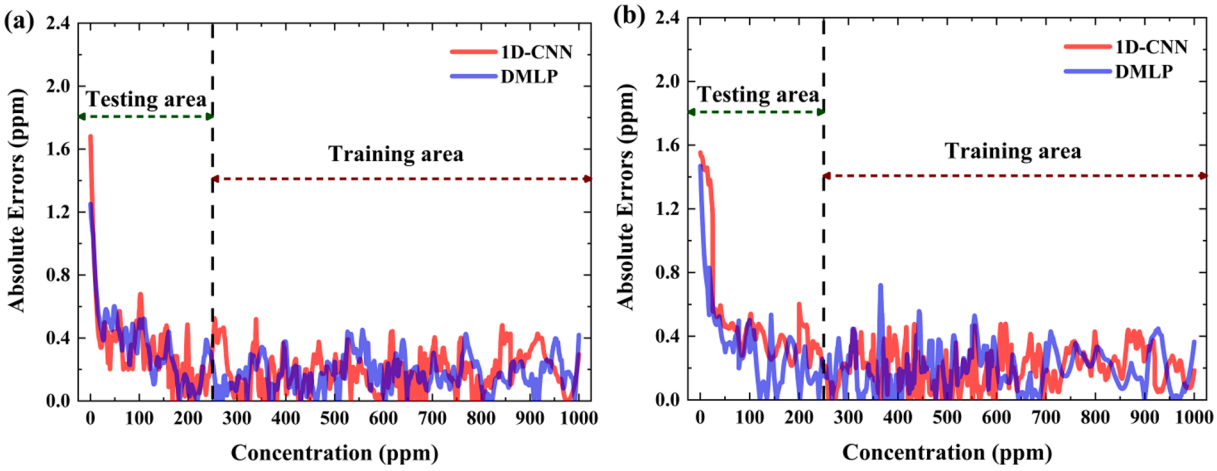

Fig. 7. Exploration errors of both DNNs for (a) methane and (b) acetylene.

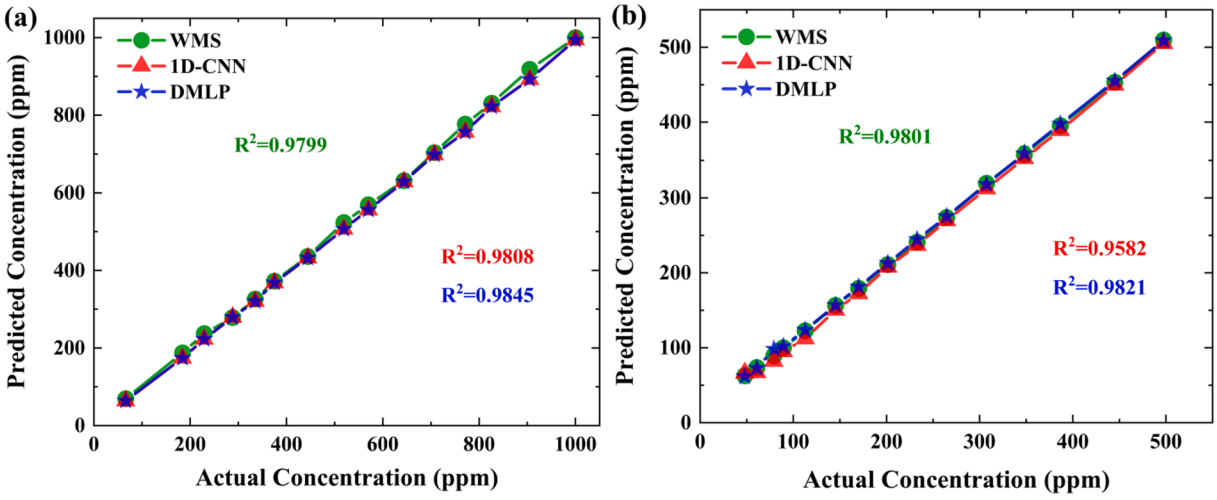

Fig. 8. The coefficients of determination comparison for (a) methane and (b) acetylene.

Table 3
Performance evaluation of DNNs based DAS gas sensor and WMS.

		1D-CNNs	DMLPs	WMS
CH_4	R^2	0.9808	0.9845	0.9799
	Relative errors (mean)/%	0.6526	0.5783	0.6826
	Relative errors (σ)/%	1.2423	1.2074	1.5888
	Absolute errors(mean)/ppm	1.2689	1.1794	1.2843
	Absolute errors(σ)/ppm	1.5982	1.0763	1.9627
C_2H_2	R^2	0.9582	0.9821	0.9801
	Relative errors (mean)/%	0.8895	0.5871	0.6081
	Relative errors (σ)/%	5.1555	1.2183	1.3749
	Absolute errors(mean)/ppm	1.5132	1.3827	1.4083
	Absolute errors(σ)/ppm	1.9823	1.1842	1.2073

The mean retrieved concentrations for both gases were close enough to the ground truth, as shown in Fig. 9(a) and (b). The reason for the fluctuation of retrieval results was that the actual gas concentration in the gas cell was not always maintained at the concentration we set due to the influence of the gas flow variation, which led to a deviation between pre-set concentration and actual concentration. Concerning the impact of light intensity attenuation on the proposed system, even the worst result still looks good to a spectroscopist, as the mean retrieved concentrations are approximate to the actual values and standard deviations are small.

We finally tested the robustness of the proposed DNNs based DAS technique to circuit parameters variations by changing the amplifier gain. Keeping the concentrations of methane and acetylene unchanged, the gain of the post-amplifier is adjusted from 1 to 50 times by adjusting the feedback resistance in the amplifier circuit. The quantitative results are shown in Fig. 9(c) and (d). The results show that the proposed technique has robustness to the moderate amplitude increase of the amplifier gain.

5. Conclusion and discussion

In summary, the main contribution of this study is to establish a basis for further research on the contacts between the deep learning algorithms with trace gas diagnosis, blended absorption features identification and separation, and so on. We demonstrate that adequate network architectures can be used to directly compute the concentration by its corresponding transmitted signal without the need for complicated optical system arrangement (e.g. WMS system) and data processing workflow (e.g. baseline fitting). Benefiting from employing the transfer learning, we tackle the difficulty of training deep learning models with limited experimental data. By comparing the performance of DNNs based DAS technique with WMS technique, we verified the satisfactory accuracy of the DNNs based gas sensor through novel evaluation methods (e.g. FCV and FH). Besides, all the DNNs based systems can deal with the problem of laser ageing and adapt to different detection systems regardless of the influence of different circuit

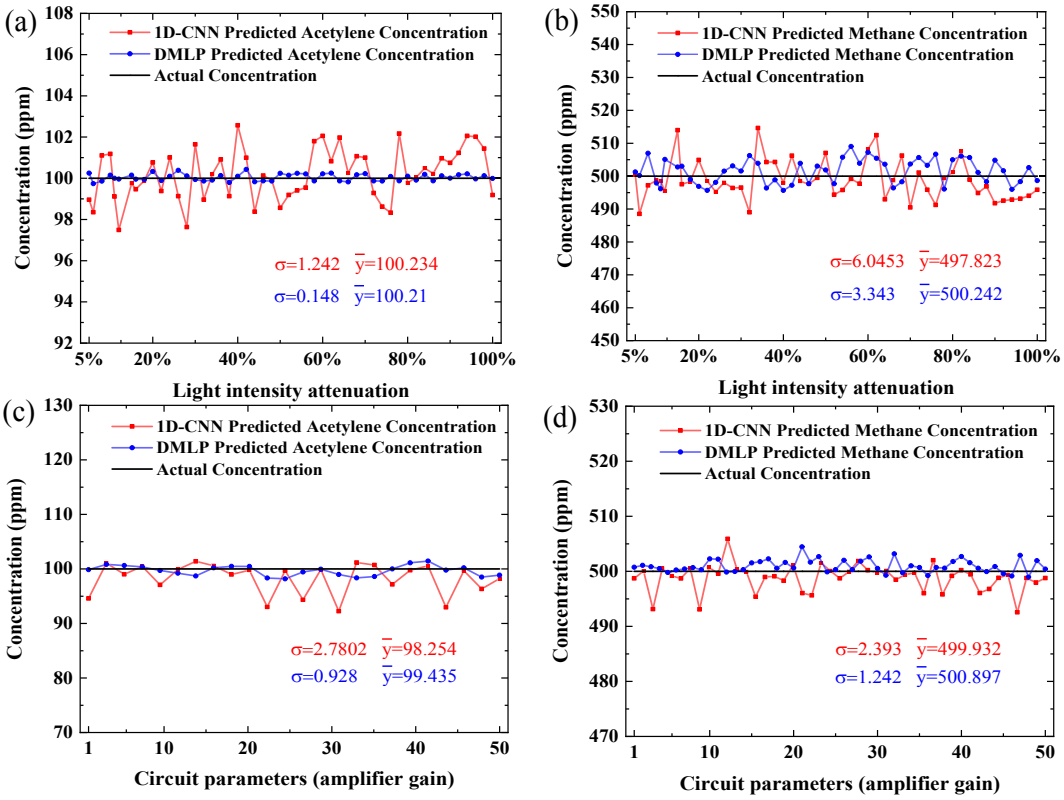

Fig. 9. The results of light intensity attenuation for (a) acetylene and (b) methane. The impact of circuit parameters variations for (c) acetylene and (d) methane.

parameters and light intensity variations. Notably, the fast computation speed and high prediction accuracy reflect the prospect of engineering application of the proposed technique. The demonstrated success of the application of deep learning in DAS indicates that the DNNs can be widely applied to various absorption spectroscopies in different context.

We believe that the application of DNNs can improve the performance of many technologies used in the diagnostics of gas spectroscopy, including blended gas recognition and trace gas measurements. Although the demand for data amount is a major drawback, we plan to further investigate the generative model[36], namely to generate more data by learning the data distribution of measured spectra. So far, the end-to-end model is the main trend of the deep learning community, the significant anticipated benefit in these cases is that it would be unnecessary to have extensive spectroscopic information as a prerequisite of the practical determination of gas detection since the DNNs should search the optimal mapping function between the input and the target automatically and minimize human intervention. But this greatly reduces the interpretability of the intermediate process in the neural networks (e.g. the proposed models in this paper can detect signals under noisy conditions accurately, unlike the filtering algorithm, the contribution to the de-noise process is not characterized). Through FCV, we also found that the current machine learning algorithms struggle to meet the requirement of gas concentration retrieval. Although our DNNs have a certain explorative power, they perform poorly in the face of low concentration signal with respect to low SNR. We hope to introduce deep learning into each gas sensing workflow in future research, so as to improve the interpretability of DNNs based gas sensing techniques as well as the robustness to noisy signals.

CRediT authorship contribution statement

Linbo Tian: Conceptualization, Investigation, Writing - original draft, Methodology, Software. **Jiachen Sun:** Conceptualization, Investigation, Writing - original draft, Methodology, Software. **Jun Chang:** Supervision, Funding acquisition, Project administration. **Jinbao Xia:** Writing - review & editing, Funding acquisition. **Zhifeng Zhang:** Writing - review & editing, Software. **Alexandre A. Kolomenskii:** Writing - review & editing. **Hans A. Schuessler:** Funding acquisition, Writing - review & editing. **Sasa Zhang:** Supervision, Funding acquisition, Project administration.

Declaration of Competing Interest

The authors declare that they have no known competing financial interests or personal relationships that could have appeared to influence the work reported in this paper.

Acknowledgments

This work was supported by National Natural Science Foundation of China (61475085), Open Fund of State Key Laboratory of Applied Optics (SKLA02020001A12) and the Robert A. Welch Foundation, grant No. A1546.

References

[1] Z. Zhang, T. Pang, Y. Yang, H. Xia, X. Cui, P. Sun, B. Wu, Y. Wnag, M.W. Sigrist, F. Dong, Development of a tunable diode laser absorption sensor for online monitoring of industrial gas total emissions based on optical scintillation cross-correlation technique, Opt Express 24 (2016) A943–A955.

[2] Y. Wang, Y. Wei, J. Chang, T. Zhang, T. Liu, T. Sun, K.T. Grattan, Tunable Diode Laser Absorption Spectroscopy-Based Detection of Propane for Explosion Early Warning by Using a Vertical Cavity Surface Enhanced Laser Source and Principle Component Analysis Approach, IEEE Sensors Journal 17 (2017) 4975–4982.

[3] V. Ebert, T. Fernholz, C. Giesemann, H. Pitz, H. Teichert, J. Wolfrum, H. Jaritz, Simultaneous diode-laser-based in situ detection of multiple species and temperature in a gas-fired power plant, Proceedings of the Combustion Institute 28 (2000) 423–430.

[4] J. Shao, Y. Zhu, S. Wang, D. Davidson, R. Hanson, A shock tube study of jet fuel pyrolysis and ignition at elevated pressures and temperatures, Fuel 226 (2018) 338–344.

[5] A. Tulgestke, S. Johnson, D. Davidson, R. Hanson, High-speed imaging of inhomogeneous ignition in a shock tube, Shock Waves 28 (2018) 1089–1095.
[6] R. Spearrin, W. Ren, J. Jeffries, R. Hanson, Multi-band infrared CO_2 absorption sensor for sensitive temperature and species measurements in high-temperature gases, Applied Physics B 116 (2014) 855–865.
[7] J. Mikołajczyk, Z. Bielecki, T. Stacewicz, J. Smulko, J. Wojtas, D. Szabra, Ł. Lentka, A. Prokopiuk, P. Magryta, Detection of Gaseous Compounds with Different Techniques, Metrology and Measurement Systems 23 (2016) 205–224.
[8] R. Ghorbani, F. Schmidt, Real-time breath gas analysis of CO and CO_2 using an EC-QCL, Applied Physics B 123 (2017).
[9] J. Weisberger, J. Richter, R. Parker, P. DesJardin, Direct absorption spectroscopy baseline fitting for blended absorption features, Appl Opt 57 (2018) 9086–9095.
[10] M. Raza, L. Ma, C. Yao, M. Yang, Z. Wang, Q. Wang, R. Kan, W. Ren, MHz-rate scanned-wavelength direct absorption spectroscopy using a distributed feedback diode laser at 2.3 μm, Optics & Laser Technology 130 (2020).
[11] J. Xia, F. Zhu, S. Zhang, A. Kolomenskii, H. Schuessler, A ppb level sensitive sensor for atmospheric methane detection, Infrared Physics & Technology 86 (2017) 194–201.
[12] H. Li, G. Rieker, X. Liu, J. Jeffries, R. Hanson, Extension of wavelength-modulation spectroscopy to large modulation depth for diode laser absorption measurements in high-pressure gases, Appl. Opt. 45 (2006) 1052–1061.
[13] S. Schilt, L. Thévenaz, P. Robert, Wavelength modulation spectroscopy: combined frequency and intensity laser modulation, Appl. Opt. 42 (2003) 6728–6738.
[14] A. Upadhyay, A. Chakraborty, Calibration-free 2f WMS with in situ real-time laser characterization and 2f RAM nulling, Opt Lett 40 (2015) 4086–4089.
[15] G. Rieker, J. Jeffries, R. Hanson, Calibration-free wavelength-modulation spectroscopy for measurements of gas temperature and concentration in harsh environments, Appl. Opt. 48 (2009) 5546–5560.
[16] J. Sun, J. Chang, F. Wang, Q. Zhang, Z. Wang, Y. Xie, Z. Zhang, Y. Feng, Tuning Efficiency of Distributed Feedback Laser Diode for Wavelength Modulation Spectroscopy, IEEE Sensors Journal 19 (2019) 9722–9727.
[17] Z. Liu, C. Zheng, T. Zhang, et al., High-precision methane isotopic abundance analysis using near-infrared absorption spectroscopy at 100 Torr, Analyst (2020).
[18] Y. Du, Z. Peng, Y. Ding, High-accuracy sinewave-scanned direct absorption spectroscopy, Optics express 26 (22) (2018) 29550–29560.
[19] S. Zhou, N. Liu, C. Shen, et al., An adaptive Kalman filtering algorithm based on back-propagation (BP) neural network applied for simultaneously detection of exhaled CO and N_2O, Spectrochimica Acta Part A: Molecular and Biomolecular Spectroscopy 223 (2019), 117332.
[20] K. Ghosh, A. Stuke, M. Todorović, et al., Deep learning spectroscopy: Neural networks for molecular excitation spectra, Advanced science 6 (9) (2019) 1801367.
[21] Jakub Nalepa, Michal Myller, Michal Kawulok, Transfer learning for segmenting dimensionally reduced hyperspectral images, IEEE Geoscience and Remote Sensing Letters 17 (7) (2019) 1228–1232.
[22] D. Hong, L. Gao, J. Yao, et al., Graph convolutional networks for hyperspectral image classification. IEEE Transactions on Geoscience and Remote Sensing, early access, 2020.
[23] D. Hong, L. Gao, N. Yokoya, et al., More diverse means better: Multimodal deep learning meets remote-sensing imagery classification. IEEE Transactions on Geoscience and Remote Sensing, early access, 2020.
[24] B. Rasti, D. Hong, R. Hang, et al., Feature Extraction for Hyperspectral Imagery: The Evolution from Shallow to Deep: Overview and Toolbox, IEEE Geoscience and Remote Sensing Magazine 8 (4) (2020) 60–88.
[25] D. Hong, N. Yokoya, G.S. Xia, et al., X-ModalNet: A semi-supervised deep cross-modal network for classification of remote sensing data, ISPRS Journal of Photogrammetry and Remote Sensing 167 (2020) 12–23.
[26] T. Zahavy, A. Dikopoltsev, D. Moss, G.I. Haham, O. Cohen, S. Mannor, M. Segev, Deep learning reconstruction of ultrashort pulses, Optica (2018) 5.
[27] S. Kleinert, A. Tajalli, T. Nagy, et al., Rapid phase retrieval of ultrashort pulses from dispersion scan traces using deep neural networks, Optics letters 44 (4) (2019) 979–982.
[28] Oviedo F, Ren Z, Sun S, et al. (2019) Fast and interpretable classification of small X-ray diffraction datasets using data augmentation and deep neural networks. npj Computational Materials, 5(1): 1-9.
[29] W.B. Park, J. Chung, J. Jung, et al., Classification of crystal structure using a convolutional neural network, IUCrJ 4 (4) (2017) 486–494.
[30] Y. LeCun, Y. Bengio, G. Hinton, Deep learning, Nature 521 (2015) 436–444.
[31] R. M. S. Ronald K.Hanson, Christopher S. Goldenstein (2016) Spectroscopy and Optical Diagnostics for Gases. Cham: Springer International Publishing, 227-253.
[32] I. Gordon, L. Rothman, C. Hill, et al., The HITRAN2016 molecular spectroscopic database, Journal of Quantitative Spectroscopy and Radiative Transfer 203 (2017) 3–69.
[33] Z. Xiong, Y. Cui, Z. Liu, et al., Evaluating explorative prediction power of machine learning algorithms for materials discovery using k-fold forward cross-validation, Computational Materials Science 171 (2020), 109203.
[34] C. Loftis, K. Yuan, Y. Zhao, et al., Lattice Thermal Conductivity Prediction Using Symbolic Regression and Machine Learning, The Journal of Physical Chemistry A (2020).
[35] Abadi M, Agarwal A, Barham P, et al. (2016) Tensorflow: Large-scale machine learning on heterogeneous distributed systems. arXiv preprint arXiv:1603.04467.
[36] I. Goodfellow, et al., Generative adversarial nets, Advances in neural information processing systems 27 (2014) 2672–2680.